**Article:**
Cownden, R. and Lucquiaud, M. (2026) An improved open-access steady state model for flue gas CO2 capture with monoethanolamine. Carbon Capture Science & Technology. 100625. ISSN: 2772-6568

https://doi.org/10.1016/j.ccst.2026.100625

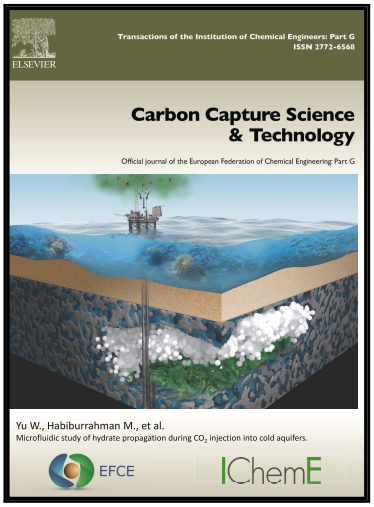


# An improved open-access steady state model for flue gas $CO_2$ capture with monoethanolamine

Ryan Cownden , Mathieu Lucquiaud

PII: S2772-6568(26)00058-8
DOI: https://doi.org/10.1016/j.ccst.2026.100625
Reference: CCST 100625

To appear in: *Carbon Capture Science & Technology*

Received date: 19 March 2026
Revised date: 8 May 2026
Accepted date: 10 May 2026

Please cite this article as: Ryan Cownden , Mathieu Lucquiaud , An improved open-access steady state model for flue gas $CO_2$ capture with monoethanolamine, *Carbon Capture Science & Technology* (2026), doi: https://doi.org/10.1016/j.ccst.2026.100625

Highlights

- Improved open-source steady state $CO_2$ capture process model for MEA
- Model validated against 4 data sources from 3 different facilities
- Laboratory equipment to large-scale pilot facilities, 75%-99% $CO_2$ capture
- More accurate $CO_2$ capture rate prediction – RMSD of 2.1 percentage points
- Versatile mass transfer correlations valid for wide range of conditions and packing

# An improved open-access steady state model for flue gas $CO_2$ capture with monoethanolamine

Ryan Cownden[1*], Mathieu Lucquiaud[1]

1. School of Mechanical, Aerospace and Civil Engineering, University of Sheffield, Sheffield, S1 3JD, UK

*Correspondence: ryan.cownden@cownden.ca

**Abstract**

The U.S. Department of Energy's Carbon Capture Simulation Initiative (CCSI) developed a "gold-standard" steady state $CO_2$ capture process model in 2018 for aqueous monoethanolamine (MEA) solvent. The CCSI model is publicly available and has been widely used for $CO_2$ capture studies. However, there are underreported issues with the model which impair its accuracy for some conditions. Here, we show how these limitations affect the accuracy of model predictions compared to large-scale pilot data and present results from an improved MEA-$CO_2$ capture model which utilises a new combination of mass transfer and thermodynamic/chemistry models. The new process model more closely predicts $CO_2$ capture rate across the wide range of process conditions and equipment scale investigated in this study. The root mean square deviation between predicted capture rate and measured data is reduced to 2.1 pp (percentage points) versus 5.3 pp using the CCSI model for 23 test cases from 3 different facilities. The accuracy improvements are particularly substantial (up to 8 pp) for emission sources with low $CO_2$ concentration, such as combined cycle gas turbines, and for absorber designs where mass transfer is not constrained by equilibrium. The Aspen Plus source file for the new process model is provided for other researchers to use and build upon.

Keywords: carbon capture, process model, monoethanolamine, $CO_2$ capture, absorption, regeneration

## 1. Introduction

Achieving the Paris Agreement climate stabilisation objectives requires urgent and ambitious reductions in anthropogenic greenhouse gas (GHG) emissions which are primarily caused by the production and consumption of fossil fuels and industrial processes (Dhakal et al., 2022). Deployment of $CO_2$ capture and storage is expected to play a substantial role in mitigating GHG emissions, particularly flue gas from large, point-source emitters such as fossil fuel power generation, steel production, and cement plants (Riahi et al., 2022).

Regenerative absorption processes using amine solvents have been widely deployed to remove $CO_2$ from process streams in industrial applications such as natural gas processing and ammonia synthesis since 1930 (Mokhatab et al., 2019, Treese, 2015). They have also been employed since 1978 for post-combustion $CO_2$ capture for merchant $CO_2$ supply (e.g., 2-117 $ktCO_2/y$ facilities in the food industry) (Chapel et al., 1999, Herzog, 1999, Fluor, 2004) and more recently at pilot facilities for $CO_2$ capture technology development – e.g., Technology Centre Mongstad (TCM) in Norway (c. 74 $ktCO_2/y$ for continuous operation) (de Koeijer et al., 2011) and the National Carbon Capture Center (NCCC) in USA (c. 3 $ktCO_2/y$) (Morton et al., 2013) – and industrial-scale power plants for GHG emissions abatement – e.g., Boundary Dam power station in Canada (c. 1 $MtCO_2/y$) (Clarke et al., 2022) and the Petra Nova project in USA (c. 1.6 $MtCO_2/y$) (Petra Nova, 2020).

Amine solvents are synthesised from ammonia by replacing one or more hydrogen atoms with hydrocarbon functional groups. Amines are attractive for $CO_2$ capture applications because they can be relatively stable, have low vapour pressure, and achieve very low residual $CO_2$ partial pressure in the outlet gas stream (Mokhatab et al., 2019). Aqueous solutions of monoethanolamine (MEA) are commonly used open-source solvents for $CO_2$ absorption, but many other open-source and proprietary amine solvent blends have been used with a range of characteristics. Amines typically absorb $CO_2$ from flue gas at low temperature (c. 40-70°C) and near atmospheric pressure in an absorption contactor and release the $CO_2$ at high temperature (c. 100-130°C) and moderate pressure (c. 1-3 barg) in a regenerator (also known as stripper/desorber) before recirculation to the absorber.

Detailed and accurate process models are crucial to facilitate deployment of $CO_2$ capture technology and establish related government policies/regulations because they are the foundation for facility design and techno-economic assessments. Rate-based process models are considered more deterministic and accurate than empirical equilibrium stage models for regenerative amine solvent absorption processes (Thompson and Tsouris, 2021). Prior studies that developed and validated amine absorption rate-based process models (e.g., Amirkhosrow et al. (2020) and Luo and Wang (2017)) have typically validated their predictions using data from laboratory-scale equipment that is several orders of magnitude smaller than equipment relevant for industrial-scale applications. Further, these laboratory tests used columns substantially shorter than typical industrial designs and focused on a relatively narrow range of column liquid fluxes that is not representative of all $CO_2$ capture applications. The mass transfer and column hydraulic models commonly used in process simulations are based on a variety of empirical relationships that deviate substantially based on fluid thermodynamic properties, packing parameters, and superficial velocities.

To help address the diversity in modelling methodologies, the U.S. Department of Energy's Carbon Capture Simulation Initiative (CCSI) developed and published a steady state $CO_2$ capture process model for aqueous MEA solvent (Soares Chinen et al., 2018). The CCSI model was developed in Aspen Plus by regressing parameters for mass transfer, column hydraulics, and reaction kinetics to minimise the differences between the process model predictions and a relatively small sample of reported laboratory-scale $CO_2$ absorber and wetted wall column data. Regression with a small sample could result in overfitting and erroneous predictions for conditions outside of the range of the regression data. Performance predicted by the CCSI model was also compared with pilot plant data from NCCC (Morgan et al., 2018), but the data was limited to flue gas from coal fired power generation which constrained the range of operating conditions. The Aspen Plus source file for the CCSI model was subsequently distributed as a standard model for post-combustion $CO_2$ capture and has been widely used for other published studies (e.g., Du et al. (2021), Michailos and Gibbins (2022), Mullen and Lucquiaud (2024), de Joannis et al. (2025)).

The CCSI model uses a variation of the Tsai correlation (Tsai et al., 2011) to determine interfacial area for mass transfer (Soares Chinen et al., 2018); this correlation is normally a function of the Weber number and Froude number. However, the dependence of interfacial area on the Froude number was omitted in the CCSI parameter regression and model validation (Morgan, 2024). This reduces the absolute value of the interfacial area calculated by the CCSI model and increases the relative dependence on liquid flux compared to the original Tsai correlation which could adversely affect the accuracy of its predictions, particularly outside of the range of liquid fluxes used in the regression (10-35 $m^3/m^2$-h).

Furthermore, the CCSI model uses a simplified chemistry model based on two reactions which does not include all ionic species (excludes $H_3O^+$, $OH^-$, and $CO_3^{2-}$) (Soares Chinen et al., 2018). The simplified reaction scheme combined with the thermodynamic parameters used in the CCSI model provide reasonable predictions of equilibrium $CO_2$ solubility in aqueous MEA for many combinations of solvent $CO_2$ loading and temperature. However, as demonstrated in this study, there are some conditions relevant for $CO_2$ capture systems where this is not the case (e.g., high solvent $CO_2$ loading and 120°C, a typical regenerator reboiler temperature).

The CCSI model is also based on a specific type of structured packing (Mellapak 250Y/252Y), whereas a wide range of packing is anticipated for different flue gas $CO_2$ capture applications. Furthermore, the CCSI model relies on parameters for kinetic, mass transfer, and hydraulic calculations that were regressed based on a limited set of experimental data (one wetted wall column study and one laboratory-scale packed bed absorber) (Soares Chinen et al., 2018).

This study presents an alternative rate-based steady state process model for flue gas $CO_2$ capture with aqueous MEA that was created to address these issues using broadly applicable mass transfer correlations developed at the University of Texas (Song et al., 2018). These mass transfer correlations are based on an extensive dataset generated with 39 different random and structured packings, including the data utilized in the original Tsai effective area correlation, and account for the effect of viscosity on the liquid mass transfer coefficient. The new process model incorporates a rigorous chemistry model which considers water/$CO_2$ ionic speciation, was validated against published vapour-liquid equilibrium data for $CO_2$-MEA-water, and includes kinetic limitations in the absorber. The new model was validated over a wider range of geometries/conditions than the CCSI model using four datasets from three different facilities – 0.1-80 $tCO_2/d$ and 4-11%mol inlet gas $CO_2$ concentration.

## 2. Methods

### *2.1 Thermodynamic property model*

The new rate-based $CO_2$ capture process model was developed in Aspen Plus using the ELECNRTL property method which combines the electrolyte non-random two liquid thermodynamic property model for the liquid phase and the Redlich-Kwong equation-of-state property model for the vapour phase (Aspen Technology Inc., 2019). This property method combination has been used to model MEA absorption of $CO_2$ in previous studies (Amirkhosrow et al., 2020), including the CCSI model (Soares Chinen et al., 2018). Henry's law is used to determine vapour-liquid equilibrium fugacity for $CO_2$, nitrogen, and oxygen. The property method is configured with the options, parameters, and databases as described in the Supplementary Material.

Model results for absorber/regenerator $CO_2$ profiles are provided as partial pressure for the vapour phase (vapour phase $CO_2$ mole fraction times total pressure) and fugacity for the liquid phase ($f_{CO2}^{L}$) which is calculated in Aspen Plus according to eqn. 1.

$$f_{CO2}^{L} = \gamma_{CO2} x_{CO2} \Phi_{CO2}^{*,v}(T, p_{CO2}^{*,l}) p_{CO2}^{*,l} \theta_{CO2}^{*,l} \quad (1)$$

Where $\gamma_{CO2}$ is the $CO_2$ activity coefficient, $x_{CO2}$ is the liquid phase $CO_2$ mole fraction, $\Phi_{CO2}^{*,v}(T, p_{CO2}^{*,l})$ is the fugacity coefficient of $CO_2$ at the system temperature and vapour pressure, $p_{CO2}^{*,l}$ is the liquid phase vapour pressure of $CO_2$ at the system temperature, and $\theta_{CO2}^{*,l}$ is the Poynting correction factor (near unity for conditions of interest for typical PCC plant applications).

### *2.2 Equilibrium chemistry*

The chemical equilibrium reactions determine the electrolytic and molecular species present in the MEA solvent and limit the extent of the kinetically controlled reactions within the

absorber unit operation. The reaction mechanism between absorbed $CO_2$ and aqueous MEA and the ionic speciation of $CO_2$/water are modelled using eqns. 2-6 (Amirkhosrow et al., 2020).

$$2H_2O \rightleftarrows H_3O^+ + OH^- \quad (2)$$

$$CO_2 + 2H_2O \rightleftarrows H_3O^+ + HCO_3^- \quad (3)$$

$$HCO_3^- + H_2O \rightleftarrows H_3O^+ + CO_3^{2-} \quad (4)$$

$$MEAH^+ + H_2O \rightleftarrows H_3O^+ + MEA \quad (5)$$

$$MEACOO^- + H_2O \rightleftarrows HCO_3^- + MEA \quad (6)$$

Equilibrium constants for each equilibrium reaction ($K_{eq}$) are unitless based on liquid phase activity (mole gamma basis) and are determined from the temperature of the liquid phase ($T_L$) according to eqn. 7 where the constant parameters $A$, $B$, $C$, $D$ are given in **Table 1**.

$$K_{eq} = \exp\left(A + \frac{B}{T_L} + \mathrm{C}\ ln(T_L) + D\ T_L\right) \quad (7)$$

Equilibrium constant parameters for the dissociation of water and $CO_2$ (reactions 2-4) are from the widely used Edwards et al. (1978) study. Equilibrium constant parameters for reactions 5-6 were regressed in this study together with the binary interaction parameters in Supplementary Table S1 using the Aspen Plus parameter regression tool and $CO_2$ solubility measurements for 15-45%wt MEA, 40-120°C, and $CO_2$ loading 0.05-0.50 $mol_{CO2}/mol_{MEA}$ reported in Aronu et al. (2011). Data from Ma'mun et al. (2005) for 30%wt MEA, 120°C, and $CO_2$ loading 0.15-0.30 $mol_{CO2}/mol_{MEA}$ was included in the regression dataset due to the lack of data in Aronu et al. for this range of solvent loading, which corresponds to typical operating conditions for regenerator reboilers in flue gas capture applications using MEA solvent (refer to Supplementary Material for additional details). The Aronu et al. dataset has a more comprehensive range of conditions than other available $CO_2$ solubility datasets and fitting the predicted vapour phase $CO_2$ partial pressure to this dataset was found to reduce the deviation between $CO_2$ capture rate predicted by the full process model and available pilot plant data. Previous studies have used a variety of equilibrium constant parameters for the dissociation of protonated MEA (reaction 4) and carbamate reversion to bicarbonate (reaction 5). We found that including the equilibrium constant parameters for these two reactions in the regression analysis reduced deviations between the model predicted vapour phase $CO_2$ partial pressure and the dataset.

**Table 1. Equilibrium constant equation parameters used in this work.** Equilibrium constant parameters for reactions 2-4 are from Edwards et al. (1978). Equilibrium constant parameters for reactions 5-6 were determined in this study using the Aspen Plus parameter regression tool and $CO_2$ solubility measurements reported in Aronu et al. (2011) and Ma'mun et al. (2005).

| reaction | A | B | C | D |
|---|---|---|---|---|
| 2 | 132.899 | -13445.9 | -22.4773 | 0 |
| 3 | 231.465 | -12092.1 | -36.7816 | 0 |
| 4 | 216.05 | -12431.7 | -35.4819 | 0 |
| 5 | -12.4751 | -5780.9 | 0 | 0.0145966 |
| 6 | -10.1504 | -270.194 | 0 | 0.0074803 |

The equilibrium vapour phase $CO_2$ partial pressure predicted by the new model shows good agreement with published measurements and provides similar results as the CCSI model with some notable exceptions where the model in this study more closely aligns with the published data (**Figure 1** for 30%wt MEA and **Supplementary Figures S1 and S2** for 15/45%wt MEA). For example, at 120°C and 30/45%wt MEA, the CCSI model predicts equilibrium vapour phase $CO_2$ partial pressure substantially higher than the range of published data for $CO_2$ loading greater than 0.40 – up to 73% higher than Aronu et al. (2011). The new model developed in this study predicts 5-14% higher $CO_2$ partial pressure for 30%wt MEA at 40°C over the full range of $CO_2$ loading from 0.05 to 0.50. Over the ranges of 40-120°C, 15-45%wt MEA, and 0.05-0.50 solvent $CO_2$ loading, the model developed in this study more closely aligns with the Aronu et al. (2011) data (refer to **Supplementary Table S3** for a detailed comparison between vapour phase $CO_2$ partial pressures predicted by the two models and reported data). The ionic species distribution predicted by the model developed in this study shows good agreement with measurements reported in Böttinger et al. (2008) – root-mean square deviation (RMSD) of 12% over 20-80°C for 30%wt MEA. The vapour-liquid equilibrium of the MEA-water binary system shows good agreement with measurements reported in Belabbaci et al. (2009) – RMSD of 7% between measured and predicted MEA vapour fraction over 20-90°C for 31.4%wt (5M) MEA. Heat of $CO_2$ absorption, an important factor in estimating regenerator energy requirements, shows good agreement with reported data at 120°C, a typical regenerator operating temperature for MEA (**Supplementary Figure S3**).

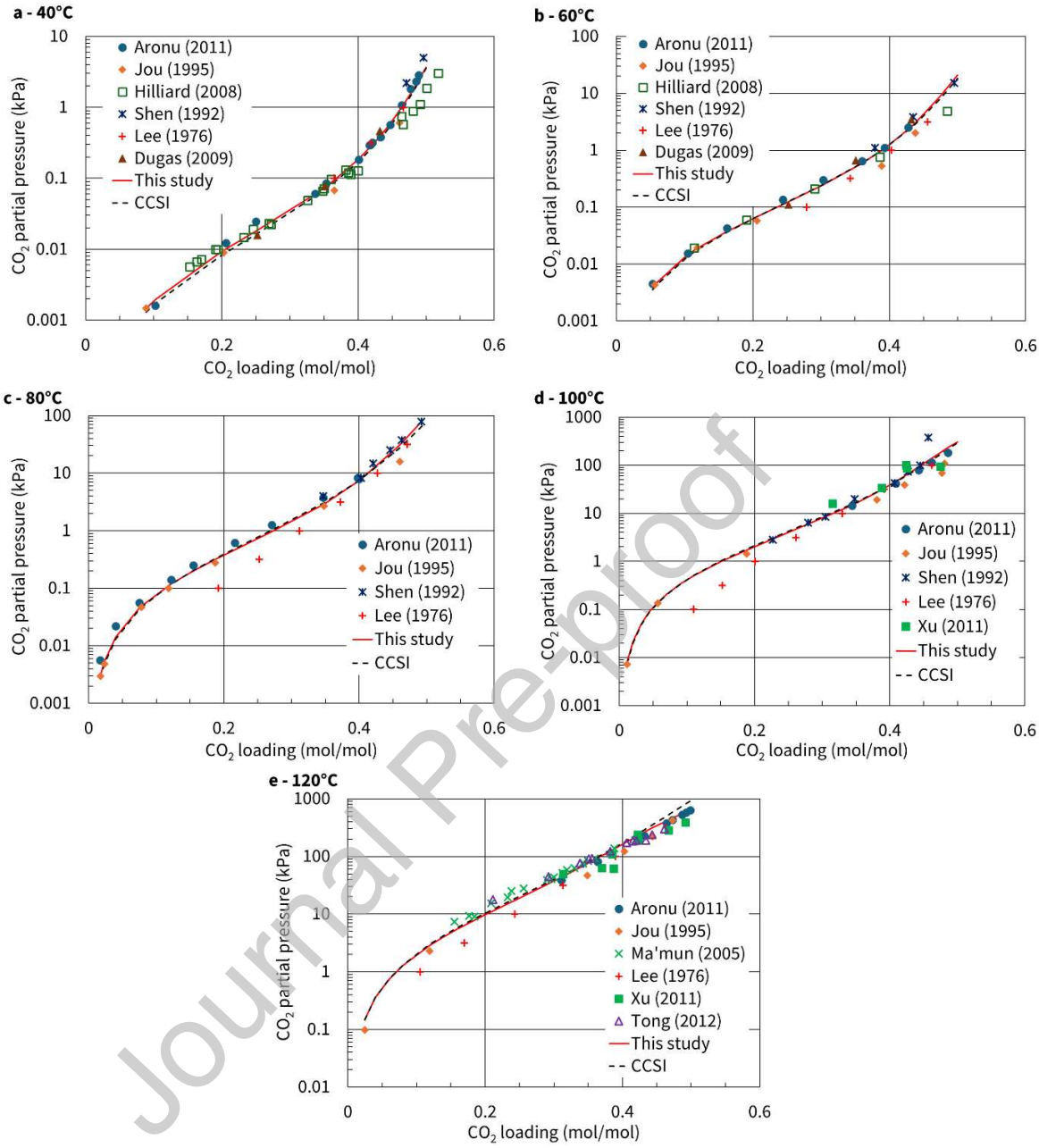




**Figure 1. Model predicted equilibrium vapour phase $CO_2$ partial pressure compared to published measurements for 30%wt MEA.** Comparison of equilibrium vapour phase $CO_2$ partial pressure versus $CO_2$ loading ($mol_{CO2}/mol_{MEA}$) predicted by the model used in this study (solid red line) and the CCSI model (dotted black line) with measurements published by Aronu et al. (2011) (solid blue circles), Jou et al. (1995) (solid orange diamonds), Hilliard (2008) (open green squares), Shen and Li (1992) (blue stars), Lee et al. (1976) corrected for the $CO_2$ loading measurement error described in Jou et al. (1995) (red crosses), Xu and Rochelle (2011) (solid green squares), Dugas and Rochelle (2009) (solid brown triangles), Ma'mun et al. (2005) (green x's), and Tong (2012) (open purple triangles) for 30%wt aqueous MEA at 40°C (**a**), 60°C (**b**), 80°C (**c**), 100°C (**d**) and 120°C (**e**).

### 2.3 Kinetically controlled reactions

The absorber is modelled assuming that the proton exchange reactions (eqns. 2, 4, and 5) follow equilibrium while the overall reactions between MEA and $CO_2$ and between $CO_2$ and hydroxide ions (eqns. 8 and 9) are kinetically limited (Amirkhosrow et al., 2020). The forward kinetic rate constants (eqns. 10 and 11) are based on Hikita et al. (1977) and Pinsent et al. (1956) respectively from the MEA-based flue gas $CO_2$ capture template available in Aspen Plus (Aspen Technology Inc., 2014, Zhang and Chen, 2013). The reverse kinetic rate constants (eqns. 12 and 13) were regressed over a temperature range of 20-80°C following the methodologies described in Zhang et al. (2009) and Amirkhosrow et al. (2020) to ensure accurate approach to equilibrium over the range of typical absorber bed temperatures. Kinetic rate constants for the absorber use a mole gamma basis with an exponent of zero for water. Similar to the CCSI model, the regenerator in this study is modelled assuming chemical equilibrium (Soares Chinen et al., 2018). Model runs completed in this study comparing predicted regenerator performance with equilibrium reactions and kinetic reactions produced nearly identical results.

$$MEA + CO_2 + H_2O \rightleftharpoons MEACOO^- + H_3O^+ \quad (8)$$

$$CO_2 + OH^- \rightleftharpoons HCO_3^- \quad (9)$$

$$k_{+8,abs} = 3.02\text{E}14\ exp\left(\frac{-4.12643\text{E}7}{R\ T_L}\right) \quad (10)$$

$$k_{+9,abs} = 1.33\text{E}17\ exp\left(\frac{-5.54709\text{E}7}{R\ T_L}\right) \quad (11)$$

$$k_{-8,abs} = 8.49\text{E}19\ exp\left(\frac{-4.778\text{E}7}{R\ T_L}\right) \quad (12)$$

$$k_{-9,abs} = 2.526\text{E}16\ exp\left(\frac{-1.050\text{E}8}{R\ T_L}\right) \quad (13)$$

Where '+' and '-' refer to the forward/reverse direction respectively for the reactions in equations 8 and 9, $R$ is the ideal gas constant (8314.46 J/kmol-K), and $T_L$ has units of K.

### 2.4 Mass transfer and liquid holdup

Mass transfer in the Aspen Plus rate-based framework is based on the two-film theory (Aspen Technology Inc., 2019). Mass transfer coefficients, interfacial area, and liquid holdup in the columns are modelled with user transport subroutines created for this study based on correlations developed by Tsai (2010) and Song et al. (2018). The mass transfer and liquid holdup correlations are based on the original regressions to retain broad validity. The liquid

and gas film mass transfer coefficients for each species $s$ ($k_{L,s}$ and $k_{G,s}$) are calculated based on eqns. 14 and 15 (Song et al., 2018).

$$k_{L,s} = 0.12 u_L^{0.565} \left(\frac{\rho_L}{\mu_L}\right)^{0.4} \frac{D_{L,s}^{0.5} g^{0.167}}{A_p^{0.065}} \left(\frac{1.8}{Z}\right)^{0.54} \quad 14$$

$$k_{G,s} = 0.28 u_G^{0.62} \left(\frac{\rho_G}{\mu_G}\right)^{0.12} D_{G,s}^{0.5} A_p^{0.38} (\sin 2\beta)^{0.65} \quad 15$$

Where $A_p$ is the specific surface area of the packing per unit volume ($m^2/m^3$), $\rho_L$ is the liquid density ($kg/m^3$), $u_L$ is superficial liquid velocity (m/s), $g$ is the acceleration of gravity (9.8067 $m/s^2$), $\mu_L$ is the liquid viscosity (Pa-s), $D_{L,s}$ is the diffusivity of species $s$ in the liquid phase ($m^2/s$), $Z$ is the height of packing elements between liquid redistribution (m), $\beta$ is the packing corrugation angle, $u_G$ is the gas superficial velocity (m/s), $\rho_G$ is the gas density ($kg/m^3$), $\mu_G$ is the gas viscosity (Pa-s), and $D_{G,s}$ is the diffusivity of species $s$ in the gas phase ($m^2/s$).

The effective interfacial area ($A_e$) of the packing is determined from eqn. 16 (Song et al., 2018).

$$A_e = 1.16 \eta A_p \left[\frac{\rho_L u_L g^{0.5}}{\sigma A_p^{1.5}}\right]^{0.138} \quad 16$$

Where the packing correction factor ($\eta$) is 1.0 for structured stainless steel packing in the pre-loading zone (<400 Pa/m pressure drop) and 1.15 in the loading zone (≥400 Pa/m pressure drop) (Song et al., 2018) and $\sigma$ is the liquid surface tension (N/m).

Liquid holdup volume ($V_L$) in each stage is calculated using eqn. 17 (Tsai, 2010).

$$V_L = 6.94 A_C z \left[\frac{u_L}{A_p S^2 g^{0.667}} \left(\frac{\mu_L}{\rho_L}\right)^{0.333}\right]^{0.573} \quad 17$$

Where $A_C$ is the packing cross sectional area ($m^2$), $z$ is the stage height (m), and $S$ is the packing channel side length (m). This liquid holdup correlation is applicable for structured packing but could be replaced with a suitable correlation for random packing to extend the methodology.

The Chilton-Colburn analogy is assumed to estimate heat transfer coefficients based on the mass transfer coefficients.

The liquid film is discretized with reactions (10 points with geometric discretization ratio of 2 based on results of Amirkhosrow et al. (2020)) and the gas film is included. A countercurrent flow model is used for the absorber (to improve temperature predictions near inlets/outlets)

and a mixed flow model is used for the regenerator (to improve model stability). A VPlug flow model can also be used for the absorber, if necessary, to improve model stability with similar (slightly lower) results for $CO_2$ capture rate prediction.

### *2.5 Pilot plant data*

This study utilises four datasets of post-combustion $CO_2$ capture with aqueous MEA solvent from three different test facilities covering a wide range of scale, process conditions, and column dimensions to validate the process model (**Table 2**): laboratory-scale data from the University of Stuttgart (Notz et al., 2012), the NCCC pilot plant (Morgan et al., 2018), and TCM (Faramarzi et al., 2017, Bui et al., 2020). A selection of 12 of 47 points in the Stuttgart dataset was used to provide a range of liquid flow rates and $CO_2$ capture rates. Raw data (Uhrig, 2025) from five stable operating conditions in the NCCC pilot plant testing described in Morgan et al. (2018) were used in this study. Additional information on the data used is available in the Supplementary Material.

**Table 2. Summary of $CO_2$ capture plant data used in this study.** Range of key process parameters and column geometry for the data used to validate the process model in this study from the University of Stuttgart (Notz et al., 2012), NCCC (Uhrig, 2025), and TCM (Faramarzi et al., 2017, Bui et al., 2020).

| | **Stuttgart** | **NCCC** | **TCM** |
|---|---|---|---|
| captured $CO_2$ ($tCO_2$/d) | 0.11-0.16 | 5.1-9.7 | 49-80 |
| absorber liquid flux ($m^3/m^2$-h) | 6.1-20 | 9.7-26 | 3.9-7.8 |
| absorber gas F-factor ($Pa^{0.5}$) | 1.6-2.1 | 1.1-2.3 | 1.3-2.7 |
| inlet gas $CO_2$ (%mol) | 5.2-10.9 | 9.0-11 | 3.6-4.1 |
| MEA mass fraction ($CO_2$-free) | 0.29-0.34 | 0.27-0.31 | 0.28-0.31 |
| lean solvent $CO_2$ loading (mol/mol) | 0.10-0.27 | 0.08-0.24 | 0.14-0.20 |
| rich solvent $CO_2$ loading (mol/mol) | 0.30-0.42 | 0.38-0.46 | 0.48-0.53 |
| $CO_2$ capture rate | 75-91% | 94-99% | 86-97% |
| regenerator reboiler duty (kW) | 6.8-17.5 | 416-436 | 2426-3323 |
| absorber packing dimensions (m) | 0.125 x 4.2 | 0.64 x 6.0-12.1 | 3.5 x 2 x 24 |
| absorber packing | Mellapak 250Y | Mellapak 252Y | Flexipac 2X |
| absorber model stages | 70 | 90 | 92 |
| regenerator packing dimensions (m) | 0.125 x 2.52 | 0.59 x 12.1 | 1.3 x 9.6 |
| regenerator packing | Mellapak 250Y | Mellapak 252Y | Flexipac 2X / Felxipac 2Y |
| regenerator model stages | 71 | 71 | 60 |
| number of data points used | 12 | 5 | 6 |

A key difference between these datasets is the height of the columns which are substantially taller in the large-scale pilot plants compared to the Stuttgart laboratory-scale plant. Taller columns more closely approach equilibrium leading to higher capture rates in the absorber and lower specific reboiler duty in the regenerator and can exhibit operating characteristics that are not present in shorter columns which are typically controlled by mass transfer rate limitations.

The $CO_2$ capture rate was calculated as the average of the four different methods described in the Supplementary Material. The Stuttgart and NCCC datasets have relatively low rich solvent $CO_2$ loading and high absorber liquid flux compared to TCM. Equilibrium $CO_2$ fugacity increases considerably at $CO_2$ loading greater than 0.40 (**Figure 1**) which can contribute to a mass transfer pinch in the absorber, while liquid flux affects the packing effective mass transfer area (Tsai et al., 2011). Temperature measurements reported for the TCM pilot plant are more thorough and robust than the other facilities because each reported value is an average of 4 measurements at that elevation distributed across the column. NCCC reports temperature measurements at a single location which is more susceptible to the effects of flow maldistribution within the packing. The Stuttgart pilot reported liquid temperatures at the redistribution points within the column which provides an average liquid temperature but at fewer locations than the TCM plant.

Each datapoint was modelled using closed-loop process simulations with the rich solvent outlet from the absorber used as input to the regenerator and the lean solvent input to the absorber adjusted to match the lean solvent loading returning from the regenerator. Closed-loop simulations were used to replicate how process models are used in the design of $CO_2$ capture plants with a priori knowledge to establish vessel geometry and operating parameters. The following reported measurements were taken as fixed inputs to the process model:

- absorber gas inlet flow, temperature, pressure, and composition
- absorber gas outlet pressure
- absorber liquid inlet flow, temperature, and MEA fraction
- regenerator rich solvent and condenser reflux inlet temperature
- regenerator pressure and heat input

The $CO_2$ capture rate in the absorber, lean solvent $CO_2$ loading, and temperature profiles in the absorber and regenerator columns predicted by the new process model and the CCSI model were compared with reported measurements. All $CO_2$ capture rates in this study refer to gross-$CO_2$ capture in the absorber (i.e., including $CO_2$ associated with ambient air used for combustion of fuel). Lean and rich solvent $CO_2$ loadings were chosen as degrees of freedom to close the loop in the process model because these measurements typically have higher uncertainty compared with other reported measurements (Morgan et al., 2018). The lean-rich cross heat exchanger was modelled for each datapoint to provide an additional check on the mass-energy balance of the reported data.

Heat loss from the regenerator is a much higher proportion of heat input for the University of Stuttgart laboratory-scale equipment compared to the larger pilot plants. Regenerator heat loss (distributed along vessel height) was adjusted in the process model for each Stuttgart

datapoint to match the predicted excess regenerator reflux condensate draw-off with the reported measurement. Heat loss was neglected for the other datasets from the larger pilot plants (and no heat loss estimates are reported with data from these plants).

## 3. Results and discussion

### *3.1 University of Stuttgart pilot data*

The $CO_2$ capture rate predicted by the new process model more closely aligns with measured data from the University of Stuttgart reported in Notz et al. (2012) than the CCSI model – RMSD of 2.8 pp v. 6.8 pp (**Figure 2**). The lean solvent $CO_2$ loading predicted by the two models are similar (RMSD of 0.015 v. 0.017 $mol_{CO2}/mol_{MEA}$); however, because of the substantial difference in predicted $CO_2$ capture, the rich solvent $CO_2$ loading predicted by the new model is closer to the reported data (RMSD of 0.016 v. 0.034 $mol_{CO2}/mol_{MEA}$). Case "Exp 17" in the data from the University of Stuttgart is the only case used in this study which was operating in the loading zone (569 Pa/m); all other cases were in the pre-loading zone.

Heat loss from the regenerator materially affects the energy balance of the Stuttgart pilot plant and the predicted lean solvent $CO_2$ loading from the regenerator. The average regenerator heat loss calculated by the new process model is 1.04 kW and 1.56 kW for the CCSI model (v. average regenerator heat input of 11.6 kW). There is substantial variability between cases for both models (0.66-1.55 kW for the new model, 1.00-2.16 kW for CCSI), which is inconsistent with the relatively stable operating temperature profile in the regenerator column between cases. Heat losses calculated by both models exceed the calculated values in Notz et al. (2012) – 0.48-1.11 kW with an average of 0.84 kW.

The largest deviations between $CO_2$ capture rate predicted by the CCSI model and the measured data are correlated with cases with higher rich solvent $CO_2$ loading (**Figure 3**). There does not appear to be a correlation between absorber liquid flux and deviations between model predicted $CO_2$ capture rates and reported measurements; however, increasing absolute magnitude of deviations between the new process model and reported measurements at liquid flux less than 12 $m^3/m^2$-h may be indicative of increasing instrumentation error and/or flow maldistribution at reduced liquid flow rates.

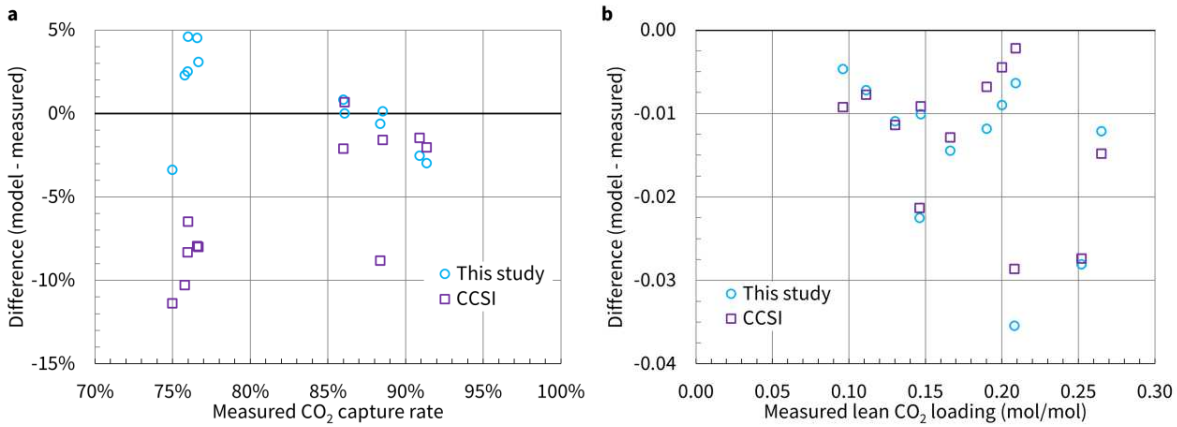


**Figure 2. Model results compared with reported data from University of Stuttgart.** Absolute difference between the $CO_2$ capture rate (panel **a**) and lean solvent $CO_2$ loading (panel **b**) predicted by the process model developed in this study (light blue circles) and the CCSI model (purple squares) and measured data reported for the University of Stuttgart laboratory facility based on the process conditions reported in Notz et al. (2012).

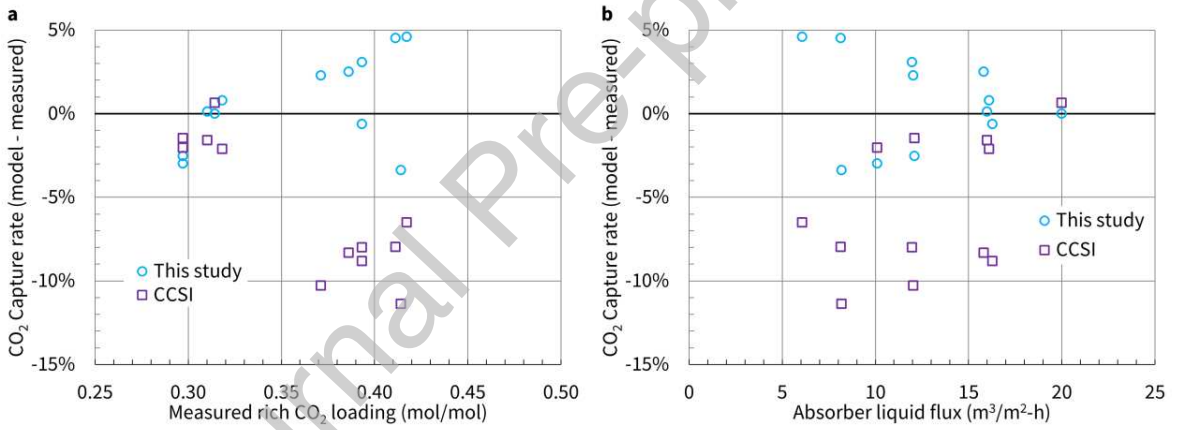


**Figure 3. Analysis of $CO_2$ capture rate deviation for University of Stuttgart data.** Absolute difference between $CO_2$ capture rate reported for the University of Stuttgart laboratory facility and the $CO_2$ capture rate predicted by the process model developed in this study (light blue circles) and the CCSI model (purple squares) versus measured rich solvent $CO_2$ loading ($mol_{CO2}/mol_{MEA}$) (panel **a**) and measured absorber liquid flux ($m^3/m^2$-h) (panel **b**). Based on the process conditions reported in Notz et al. (2012).

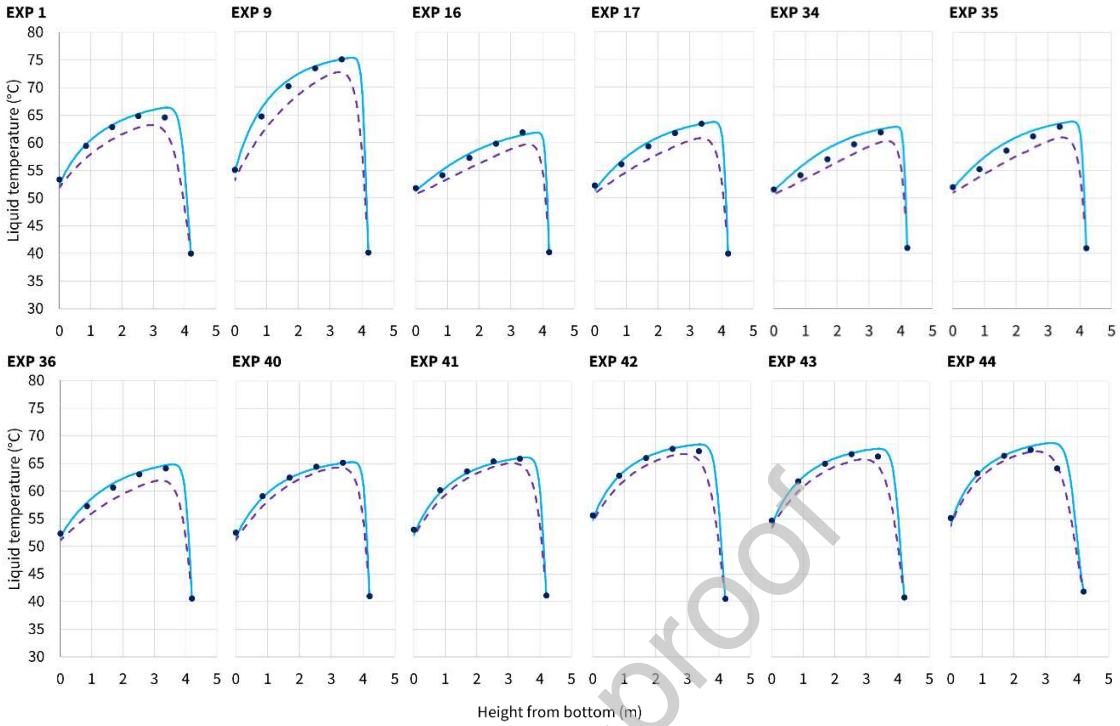


**Figure 4. Model predicted absorber temperature profiles compared with reported data from University of Stuttgart.** Liquid temperature profile in the absorber predicted by the process model developed in this study (solid light blue lines) and the CCSI model (dashed purple lines) compared with measured data (dark blue circles) reported in Notz et al. (2012). Figure panel labels refer to case numbers in Notz et al. (2012).

The absorber temperature profiles predicted by the new process model are closer to the reported data than the CCSI model for the operating conditions in Notz et al. (2012) (**Figure 4**) – overall RMSD for the 12 test conditions of 0.9°C versus 1.8°C for the CCSI model. The new process model and the CCSI model both predict regenerator temperature profiles very similar to the data reported in Notz et al. (2012) – overall RMSD over the 12 test conditions of 0.9/0.8°C respectively (**Figure 5**). The reported accuracy of the temperature measurements in Notz et al. (2012) is 0.1°C.

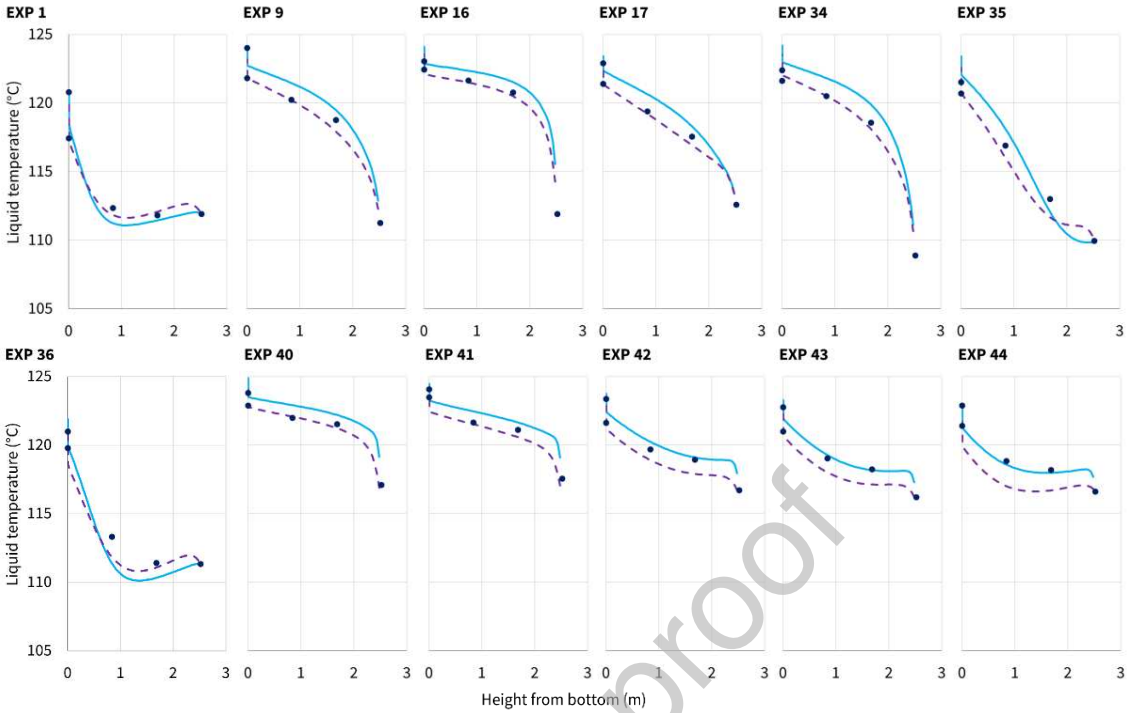


**Figure 5. Model predicted regenerator temperature profiles compared with reported data from University of Stuttgart.** Liquid temperature profile in the regenerator predicted by the process model developed in this study (solid light blue lines) and the CCSI model (dashed purple lines) compared with measured data (dark blue circles) reported in Notz et al. (2012). Figure panel labels refer to case numbers in Notz et al. (2012).

### *3.2 NCCC pilot data*

The new process model and the CCSI model both accurately predict $CO_2$ capture rates and lean solvent $CO_2$ loadings for the NCCC operating conditions (**Figure 6**) – RMSD of 1.1 pp and 0.007 $mol_{CO2}/mol_{MEA}$ respectively for the new model versus 1.4 pp and 0.005 $mol_{CO2}/mol_{MEA}$ for the CCSI model. The differences in RMSDs for $CO_2$ capture rate and lean solvent $CO_2$ loading between the two models for the NCCC cases are not significant relative to expected measurement uncertainties in the reported data.

The new process model more accurately predicts the absorber temperature profiles for the NCCC data than the CCSI model with a RMSD of 4.0°C v. 8.0°C (**Figure 7**). The new model provides a considerably more accurate prediction of absorber temperature profile for case NCCC-3 and more accurately predicts the temperature rise near the bottom of the absorber for 3 of the other 4 cases. The two models predict similar regenerator temperature profiles which closely align with the reported data – RMSDs of 1.3°C for both models (**Figure 8**). Both models consistently overpredict the regenerator temperature profile by approximately 2°C in case

NCCC-5. Differences between the regenerator temperature profiles predicted by the model are not significant relative to expected measurement uncertainties in the reported data.

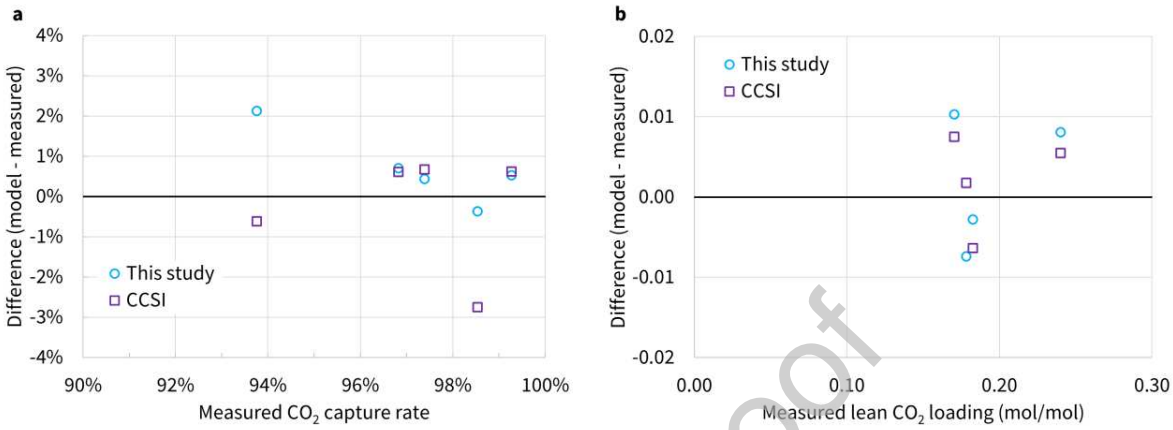


**Figure 6. Model results compared with reported data from NCCC.** Absolute difference between the $CO_2$ capture rate (panel **a**) and lean solvent $CO_2$ loading (panel **b**) predicted by the process model developed in this study (light blue circles) and the CCSI model (purple squares) and measured data reported for the NCCC pilot facility (Uhrig, 2025).

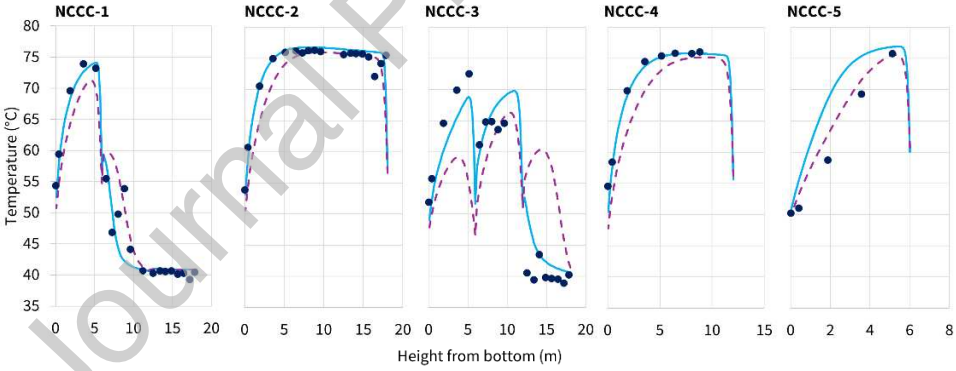


**Figure 7. Model predicted absorber temperature profiles compared with reported data from NCCC.** Interface temperature profile in the absorber predicted by the process model developed in this study (solid light blue lines) and the CCSI model (dashed purple lines) compared with measured data (dark blue circles) reported for the NCCC pilot facility (Uhrig, 2025).

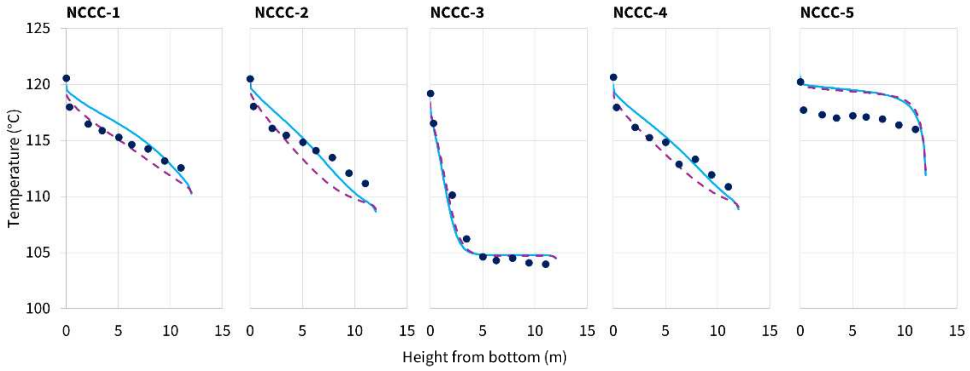


**Figure 8. Model predicted regenerator temperature profiles compared with reported data from NCCC.** Interface temperature profile in the regenerator predicted by the process model developed in this study (solid light blue lines) and the CCSI model (dashed purple lines) compared with measured data (dark blue circles) reported for the NCCC pilot facility (Uhrig, 2025).

### *3.3 TCM pilot data*

The $CO_2$ capture rate and lean solvent $CO_2$ loading predicted by the new process model more closely align with the measured data from TCM reported in Faramarzi et al. (2017) and Bui et al. (2020) (**Figure 9**) – RMSD of 1.0 pp and 0.011 $mol_{CO2}/mol_{MEA}$ for the new model respectively versus 3.3 pp and 0.024 $mol_{CO2}/mol_{MEA}$ for the CCSI model. In particular, the CCSI model overpredicted $CO_2$ capture rate by 2.5-4.9 pp for datapoints with high rich solvent $CO_2$ loading (>0.485 $mol_{CO2}/mol_{MEA}$ as predicted by the models). Two factors contributing to the higher capture rate predicted by the CCSI model in these four cases are (1) lower equilibrium $CO_2$ fugacity at high $CO_2$ loading (>0.40 $mol_{CO2}/mol_{MEA}$) and the absorber temperature in the TCM process conditions (c. 40-60°C), and (2) lower lean solvent $CO_2$ loading exiting the regenerator despite similar or higher rich solvent $CO_2$ loading leaving the absorber. Despite the increased dependence of interfacial area on liquid flux in the CCSI model due to the omission of the Froude number in the liquid mass transfer coefficient correlation, the relative reduction in the Aspen Plus liquid phase "overall binary mass transfer coefficients" (product of interfacial area, mass transfer coefficient, and molar density) calculated by the CCSI model at lower liquid flux was smaller than the new process model because of higher sensitivity of the mass transfer coefficient to liquid flux in the correlation used in the new model.

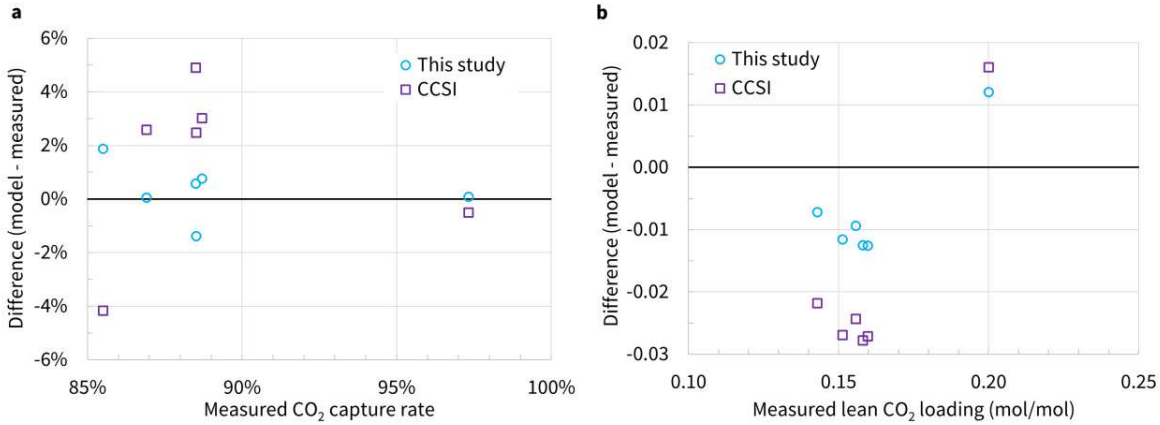


**Figure 9. Model results compared with reported data from TCM.** Absolute difference between the $CO_2$ capture rate (panel **a**) and lean solvent $CO_2$ loading (panel **b**) predicted by the process model developed in this study (light blue circles) and the CCSI model (purple squares) and measured data reported for the TCM pilot facility based on the process conditions reported in Faramarzi et al. (2017) and Bui et al. (2020).

The new process model more accurately predicts the temperature profile in the absorber (**Figure 10**) for the TCM operating conditions reported in Faramarzi et al. (2017) and Bui et al. (2020) than the CCSI model – overall RMSD over the six test conditions of 1.3°C in this study versus 3.4°C for the CCSI model. The new process model predicts a regenerator temperature profile very similar to the CCSI model for the 5 test points in Bui et al. (2020) but is closer to the data reported in Faramarzi et al. (2017) resulting in a slight improvement in overall RMSD over the six test conditions of 2.0°C versus 2.2°C (**Figure 11**).

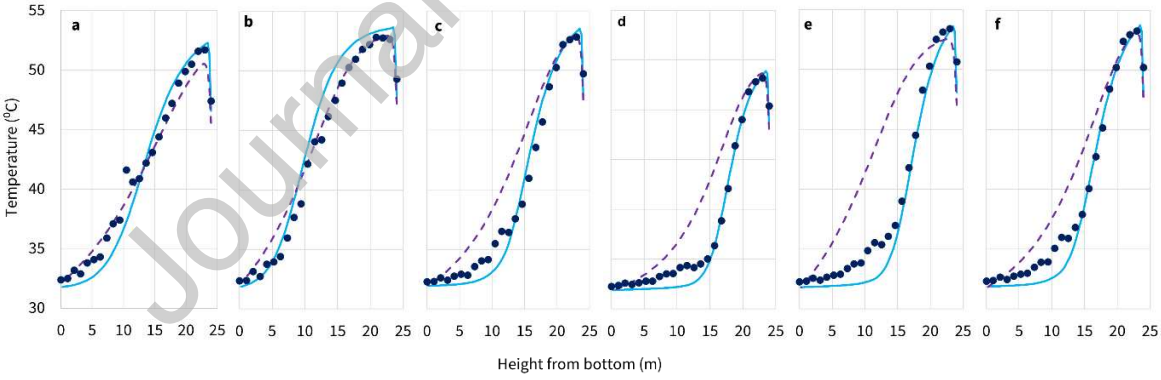


**Figure 10. Model predicted absorber temperature profiles compared with reported data from TCM.** Interface temperature profile in the absorber predicted by the process model developed in this study (solid light blue lines) and the CCSI model (dashed purple lines) compared with measured data (dark blue circles) reported for the TCM pilot facility in Faramarzi et al. (2017) (panel **a**) and test cases ICL_7 (**b**), ICL_9 (**c**), ICL_11 (**d**), ICL_12 (**e**), and ICL_13 (**f**) in Bui et al. (2020).

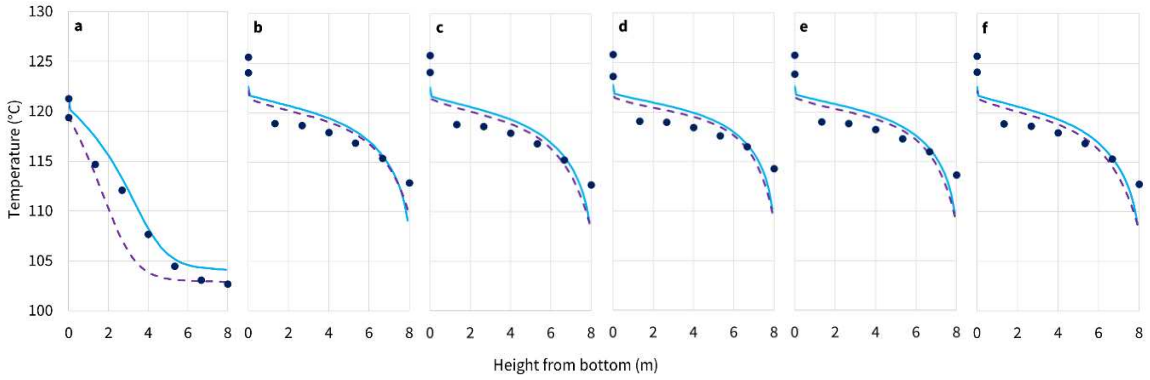


**Figure 11. Model predicted regenerator temperature profiles compared with reported data from TCM.** Interface temperature profile in the regenerator predicted by the process model developed in this study (solid light blue lines) and the CCSI model (dashed purple lines) compared with measured data (dark blue circles) reported for the TCM pilot facility in Faramarzi et al. (2017) (panel **a**) and test cases ICL_7 (**b**), ICL_9 (**c**), ICL_11 (**d**), ICL_12 (**e**), and ICL_13 (**f**) in Bui et al. (2020).

### *3.4 Summary of pilot plant comparisons*

The new process model provides similar or improved predictions of $CO_2$ capture rate and lean solvent $CO_2$ loading for all the datasets assessed (**Table 3**). The overall RMSD for $CO_2$ capture rate for all 23 datapoints is 2.1 pp for the new model compared to 5.3 pp for the CCSI model. The overall RMSD for lean solvent $CO_2$ loading is similar for the new model and CCSI model (0.014 and 0.017 $mol_{CO2}/mol_{MEA}$ respectively). Absorber temperature profiles predicted by the new model more closely align with the data reported for the Stuttgart, NCCC, and TCM pilot plants while the regenerator temperature profiles predicted by the two models are similar.

**Table 3. Summary of RMSDs between model predicted values and reported measurements.** RMSDs for $CO_2$ capture rate, lean solvent $CO_2$ loading, and absorber/regenerator temperature profiles predicted by the process model developed in this study and the CCSI process model compared to measurements reported for the Stuttgart laboratory pilot (Notz et al., 2012), the NCCC pilot plant (Morgan et al., 2018), and the TCM pilot plant (Faramarzi et al., 2017, Bui et al., 2020).

| dataset/model | $CO_2$ capture rate (pp) | lean $CO_2$ loading ($mol_{CO2}/mol_{MEA}$) | absorber temperature profile (°C) | regenerator temperature profile (°C) |
|---|---|---|---|---|
| **Stuttgart** | | | | |
| new model | 2.8 | 0.017 | 0.9 | 0.9 |
| CCSI | 6.8 | 0.015 | 1.8 | 0.8 |
| **NCCC** | | | | |
| new model | 1.1 | 0.007 | 4.0 | 1.3 |
| CCSI | 1.4 | 0.005 | 8.0 | 1.3 |
| **TCM** | | | | |
| new model | 1.0 | 0.011 | 1.3 | 2.0 |
| CCSI | 3.3 | 0.024 | 3.4 | 2.2 |

### *3.4.1 University of Stuttgart*

The mass transfer and chemistry parameters in the CCSI model were regressed using wetted wall column data (Dugas, 2009) and laboratory-scale absorber data (Tobiesen et al., 2007). The Tobiesen et al. (2007) data included 20 points over a liquid flux range of 10-31 $m^3/m^2$-h and many points with rich solvent loading lower than the range anticipated for economically viable $CO_2$ capture plants (12 of 20 points <0.35 $mol_{CO2}/mol_{MEA}$, only 2 of 20 points >0.44 $mol_{CO2}/mol_{MEA}$). Similar to the University of Stuttgart pilot plant, Tobiesen et al. used a shorter absorber column (4.4 m) than commercial-scale absorbers and achieved low $CO_2$ capture rates (all 20 points <86%, 19 of 20 points <81%). Interphase $CO_2$ mass transfer rates under these conditions are not strongly affected by bulk liquid equilibrium/kinetic limitations. Within that range of liquid flux and low rich solvent loading, the CCSI model and the new process model produce similar results that generally align with reported measurements. Outside of those ranges some important deviations develop under certain operating conditions.

For rich solvent $CO_2$ loading >0.35 $mol_{CO2}/mol_{MEA}$, the CCSI model underpredicted $CO_2$ capture rate by 7-11 pp while the new model aligned with the reported data within -3/+5 pp. The CCSI model predicted lower mass transfer due to calculated interfacial area (c. 20-30% lower, correlation omitting Froude number dependence) and liquid mass transfer coefficients (c. 80-90% lower) substantially lower than the new model. The CCSI model uses the Billet and Schultes correlation for mass transfer coefficients with the $C_L/C_G$ constants and binary diffusion coefficients regressed to fit the Dugas (2009) and Tobiesen et al. (2007) data (Soares Chinen et al., 2018). The CCSI model predicts lower concentration of unreacted MEA at the interface than the new model leading to higher solvent $CO_2$ fugacity (**Figure 12**). The limitation to interphase $CO_2$ transfer in the CCSI model in these cases is the concentration gradient between the bulk liquid and the interface. Reaction kinetics are strongly dependent on MEA concentration in the CCSI model which amplifies the effect on $CO_2$ mass transfer for cases with higher solvent $CO_2$ loading (e.g., 0.39 $mol_{CO2}/mol_{MEA}$ in EXP36 v. 0.30 $mol_{CO2}/mol_{MEA}$ in EXP41). Furthermore, cases with higher capture rate (e.g., 91% in EXP41) have lower $CO_2$ flux near the top of the absorber due to depletion of vapour phase $CO_2$ which mitigates the effect of differences in the mass transfer coefficients. Bulk liquid $CO_2$ fugacity away from the vapour-liquid interface remains low with the Stuttgart operating conditions.

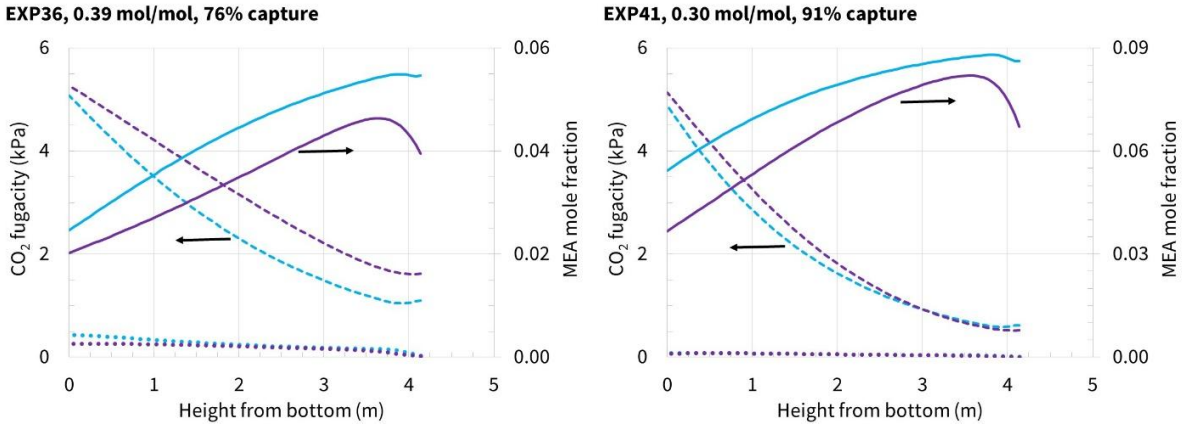


**Figure 12. Model predicted absorber composition profiles for Stuttgart cases.** Profiles of liquid MEA mole fraction at the interface (solid lines, RHS), solvent $CO_2$ fugacity at the interface (dashed lines, LHS), and bulk solvent $CO_2$ fugacity (dotted lines, LHS) in the absorber predicted by the process model developed in this study (light blue lines) and the CCSI model (purple lines) for Stuttgart test cases EXP36 and EXP41 in Notz et al. (2012). Liquid/gas flow rates and inlet gas $CO_2$ concentration are similar in the two cases, but EXP36 has higher rich solvent $CO_2$ loading than EXP41 (0.39 v. 0.30 $mol_{CO2}/mol_{MEA}$) and lower $CO_2$ capture (76% v. 91%).

### *3.4.2 NCCC*

The binary mass transfer coefficients calculated by the new model for the NCCC pilot plant data were higher than the CCSI model by a factor of approximately 3-4. Yet the overall capture rate predictions were similar in most cases because interphase $CO_2$ mass transfer was constrained by the vapour phase $CO_2$ approaching the bulk solvent equilibrium $CO_2$ fugacity at the top of the absorber (**Figure 13**).

For the NCCC-3 and NCCC-5 cases, the CCSI model predicted a $CO_2$ capture rate c. 3 pp lower than the new model. In both cases this was due to lower concentration of unreacted MEA at the interface leading to increased solvent $CO_2$ fugacity for the reasons discussed in Section 3.4.1. While the capture rate and absorber temperature profile predicted by the new model more closely aligned with the reported data for the NCCC-3 case, the CCSI model results more closely matched the reported data for the NCCC-5 case. This divergence indicates that other factors such as flow distribution may be contributing to the reported results (case NCCC-5 had considerably lower solvent flow rate than any of the other NCCC cases).

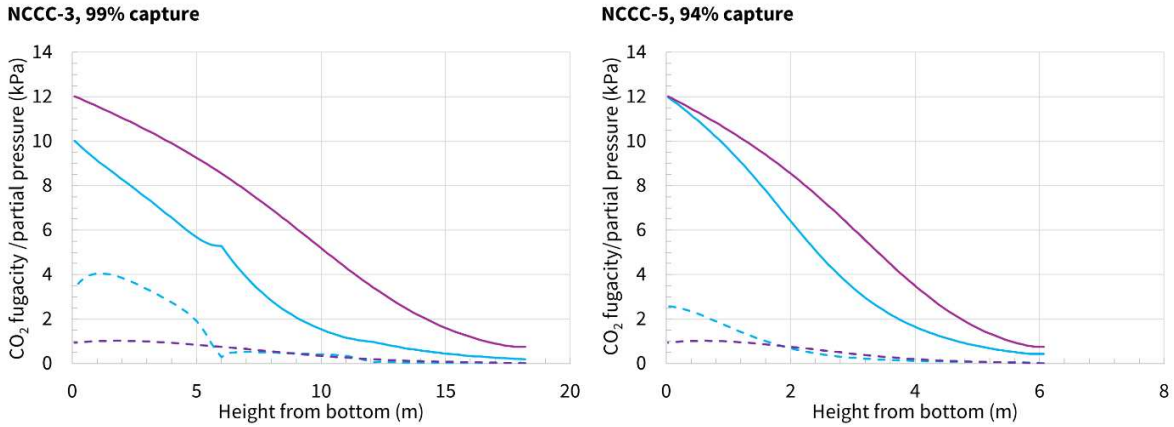


**Figure 13. Model predicted absorber $CO_2$ profiles for NCCC cases.** Vapour $CO_2$ partial pressure (solid lines) and bulk liquid $CO_2$ fugacity (dashed lines) profiles in the absorber predicted by the process model developed in this study (light blue lines) and the CCSI model (purple lines) for the NCCC-3 (left panel) and NCCC-5 (right panel) conditions.

Case NCCC-5 had the lowest lean solvent loading (0.075 $mol_{CO2}/mol_{MEA}$) in the validation dataset. Both models predicted lean loading consistent with reported data (within c. 0.01 $mol_{CO2}/mol_{MEA}$ deviation) but overpredicted the temperature profile through the entire regenerator. This test point has substantially lower solvent flow rate than the other four cases (3390 kg/h v. 7081-9370 kg/h rich solvent) which may have contributed to flow maldistribution in the regenerator. Nonetheless, there is very little published vapour-liquid equilibrium data available at typical regenerator temperatures (100-120°C) and solvent $CO_2$ loading less than 0.15 $mol_{CO2}/mol_{MEA}$ to validate chemistry models for MEA-$CO_2$-water – 3 measurements each at 100/120°C and 30%wt MEA, 1 measurement each at 100/120°C and 15%wt MEA, and 1 measurement at 120°C and 45%wt MEA. This gap in published equilibrium data is notable because recent studies have advocated operating post-combustion $CO_2$ absorbers with lean solvent loading <0.15 $mol_{CO2}/mol_{MEA}$ to reduce the energy penalty associated with achieving a high $CO_2$ capture rate (Michailos and Gibbins, 2022, Mullen and Lucquiaud, 2024). The cases in the validation dataset with lean solvent loading closest to NCCC-5 were EXP16 and EXP40 from the University of Stuttgart (0.10 and 0.11 $mol_{CO2}/mol_{MEA}$ respectively). The regenerator temperature profiles predicted by both models for these cases closely aligned with the reported data.

### *3.4.3 TCM*

Lower lean solvent loading calculated by the CCSI regenerator model compared to the new process model accounts for approximately half of the $CO_2$ capture overprediction by the CCSI model for the TCM cases. The rich solvent MEA is nearly depleted based on reaction stoichiometry. Capture rate in this condition is approximately a linear function of predicted lean solvent loading.

However, the CCSI model also predicts faster reaction kinetics in the absorber than the new model which reduces the predicted solvent $CO_2$ fugacity and leads to higher predicted mass transfer. **Figure 14a** provides the profile of solvent $CO_2$ fugacity and vapour $CO_2$ partial pressure predicted in the absorber for Case ICL_11 in Bui et al. (2020). The equilibrium solvent $CO_2$ fugacity downstream of the absorber in the two models is very similar (c. 1.5 kPa). However, the new process model predicts slower MEA-$CO_2$ reaction kinetics leading to solvent $CO_2$ fugacity considerably higher than equilibrium within the packing and a mass transfer pinch near the bottom of the absorber. This result contrasts with the Stuttgart data where bulk liquid $CO_2$ fugacity remained low due to higher temperature in the absorber packing and smaller increase in solvent $CO_2$ loading in the short absorber column. Faster kinetics also explain the higher deviations in temperature profile in the lower portion of the absorber for the CCSI model compared to reported TCM measurements because the increased rate of $CO_2$ absorption near the bottom of the column increases the temperature profile in that part of the tower. This reaction kinetics effect is not apparent in the NCCC data because the substantially higher inlet gas $CO_2$ concentration – 9.0-11.0%mol v. 3.6-4.1%mol in the TCM data – reduces the significance of deviations in the predicted solvent $CO_2$ fugacity to the mass transfer calculations. Higher inlet gas $CO_2$ concentration also leads to higher absorber bed temperature than the TCM cases which increases the reaction rates such that they do not materially constrain interphase $CO_2$ transfer.

The CCSI model predicts slightly more $CO_2$ flashing off prior to the regenerator inlet and more rapid approach between liquid and vapour $CO_2$ fugacity than the new model. This causes lower predicted outlet lean solvent loading with the regenerator heat input fixed based on the reported data (**Figure 14b**). The CCSI model uses the same mass transfer model parameters in the regenerator that were regressed based on MEA-$CO_2$ absorber data.

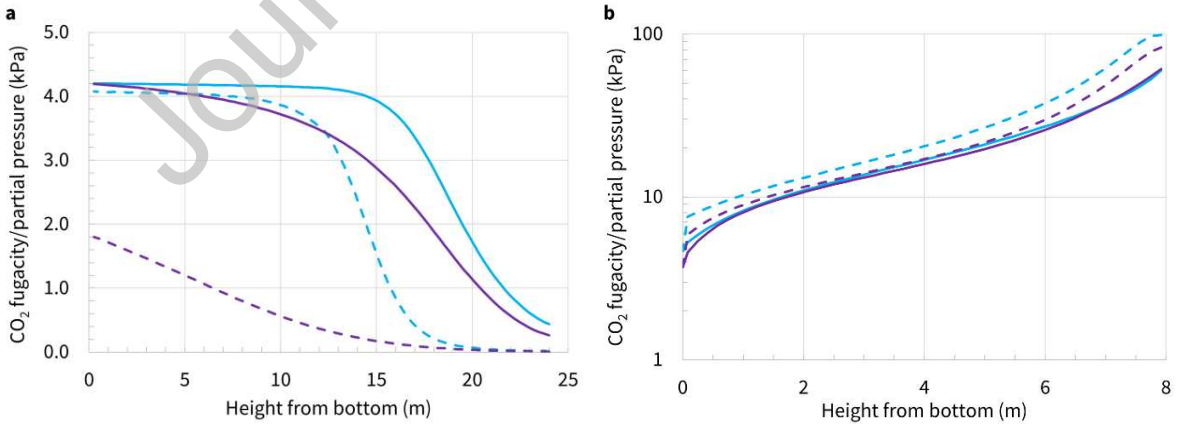


**Figure 14. Model predicted absorber and regenerator $CO_2$ profiles for TCM case.** Vapour $CO_2$ partial pressure (solid lines) and bulk liquid $CO_2$ fugacity (dashed lines) profiles in the absorber (panel **a**) and regenerator (panel **b**) predicted by the process model developed in this study (light blue lines) and the CCSI model (purple lines) for the ICL_11 test conditions in Bui et al. (2020).

### *3.5 Other mass transfer and chemistry models*

Numerous different permutations of mass transfer and chemistry models were investigated during development of the new process model. The effect of different chemistry models on the predicted $CO_2$ capture rate and column temperature profiles was found to be more important for the larger pilot plant conditions than the laboratory-scale data due to closer approach to equilibrium and/or kinetic limitations. This was particularly the case for test cases with high rich solvent $CO_2$ loading. Published $CO_2$ solubility data for aqueous MEA exhibits a substantial range (e.g., c. ±30% at 40°C and 30%wt. MEA); however we found that mass transfer pinches demonstrated in large-scale pilot plants could best be predicted by models approximating the data published in Aronu et al. (2011) which also resulted in $CO_2$ fugacity predictions similar to the CCSI model for many, but not all, conditions. Similar to Amirkhosrow et al. (2020) and Zhang et al. (2009), we found that it was possible to create process models based on the Bravo-Rocha-Fair mass transfer correlations (Bravo et al., 1985) (e.g., with the CCS template model provided in the Aspen Plus example library) which reasonably matched laboratory-scale absorber data and that these correlations more closely aligned with the reported data than other standard correlations available in Aspen Plus (e.g., Billet and Schultes (1999)); however, the results from these models aligned poorly with the large-scale pilot data used in this study when those models were scaled up.

## 4. Conclusion

Accurate models for regenerative amine absorption processes are important to support development and deployment of $CO_2$ capture and storage as a key technology to mitigate GHG emissions. The widely used CCSI model for MEA-based $CO_2$ capture was developed by matching performance from laboratory-scale equipment which can lead to bias and inaccuracy in model predictions due to process conditions and geometry which deviate from industrial-scale equipment. An improved flue gas $CO_2$ capture process model for aqueous MEA has been developed and validated against pilot plant data from three different facilities covering a wide range of compositions (3.6-11%mol inlet gas $CO_2$ concentration and 0.08-0.27 $mol_{CO2}/mol_{MEA}$ lean solvent loading), liquid fluxes (3.9-26 $m^3/m^2$-h), $CO_2$ capture rates (75-99%), and geometries, including column heights that are representative of commercial equipment (up to 24 m in the absorber and 12 m in the regenerator). The new process model includes regressed thermodynamic and chemistry parameters which improve the prediction of $CO_2$ partial pressure for 15-45%wt MEA and 40-120°C compared to the incumbent standard model for aqueous MEA absorption of $CO_2$ (CCSI).

The new model more closely aligns with pilot plant data than the CCSI model – overall RMSD for $CO_2$ capture rate of 2.1 pp for the new model compared to 5.3 pp for the CCSI model. The mass transfer and kinetic correlations which were regressed for the CCSI model based on a limited set of wetted wall column and laboratory-scale absorber data result in predictions which substantially deviate from reported data for some conditions. The new model particularly improves the accuracy of predictions for cases involving high rich solvent loading (>0.40 $mol_{CO2}/mol_{MEA}$) combined with low vapour $CO_2$ partial pressure and industrial height columns where equilibrium and kinetic limitations to mass transfer become more significant. The new process model substantially improves the accuracy of predicted performance for applications with low absorber operating temperature (<50°C) where reaction kinetics can be an important limitation and short absorber columns where interface mass flux limits $CO_2$ transfer. The new model is also more versatile with respect to packing type than the CCSI model because it is not constrained by a parameter regression based on a small dataset and a single structured packing.

These improvements are of particular significance for modelling and optimising process designs for high $CO_2$ capture from industrial scale combined cycle gas turbines which typically have flue gas $CO_2$ concentration comparable to the TCM test case conditions. Small differences in predicted capture rate could result in substantial differences in absorber height required to achieve a high $CO_2$ capture design requirement because of the reduced mass transfer driving force available as the flue gas $CO_2$ depletes. Accurately predicting absorber size is critical for PCC technoeconomic analyses because the absorber accounts for approximately 43% of the capital cost for a typical MEA-based flue gas $CO_2$ capture plant (Barlow et al., 2025). The improved accuracy in predicting interphase $CO_2$ transfer at low temperature with the new model will be crucial for determining optimal absorber design temperatures and assessing the performance of intercooling.

Furthermore, emerging regulations for $CO_2$ capture plants will require project proponents to ensure that their plant designs achieve high $CO_2$ capture rates. Compliance with the Canadian Clean Electricity Regulation and UK permitting requirements for PCC plants requires >95% $CO_2$ capture from combined cycle gas turbines (Government of Canada, 2024, UK Environment Agency, 2024). Accurate PCC process models will improve confidence in predicted capture rates and mitigate the risk of PCC plants failing to meet regulatory requirements.

A copy of the Aspen Plus source file is included with the Supplementary Material to facilitate use and improvement of this model by other researchers.

**List of abbreviations**

CCSI Carbon Capture Simulation Initiative

NCCC National Carbon Capture Center

TCM Technology Centre Mongstad

**Supplementary material**

Aspen Plus source file. Detailed information on Aspen Plus model configuration, extended model $CO_2$ fugacity predictions, and pilot plant data used in the analysis.

**Data availability**

A copy of the Aspen Plus model that was developed in this research and was used to generate the results is included in the Supplementary Material (Version 11 and 14). The Supplementary Material also provides detailed information on the pilot plant data used for the model validation and source references.

**Author contributions**

Ryan Cownden: conceptualization, methodology, investigation, validation, formal analysis, data curation, visualization, writing – original draft, writing – review and editing. Mathieu Lucquiaud: conceptualization, methodology, writing – review and editing, supervision, resources.

**Acknowledgements**

The authors would like to acknowledge funding from the University of Sheffield and the Natural Sciences and Engineering Research Council of Canada (NSERC), [funding reference number 566581109] which supported this research. The authors would also like to acknowledge funding from the University of Sheffield Institutional Open Access Fund which supported publication of this article. The authors are grateful for the cooperation of Tony Wu and Laura Uhrig from the Southern Company which provided data from the National Carbon Capture Center (supported by the US Department of Energy under Award Number DE-FE0022596) that was used in this study for model validation.



**Declaration of competing interest**

The authors declare that they have no known competing financial interests or personal relationships that could have appeared to influence the work reported in this paper.

**References**

AMIRKHOSROW, M., PÉREZ-CALVO, J.-F., GAZZANI, M., MAZZOTTI, M. & NEMATI LAY, E., 2020. Rigorous rate-based model for CO2 capture via monoethanolamine-based solutions: effect of kinetic models, mass transfer, and holdup correlations on prediction accuracy. *Sep. Sci. Technol.,* 56**,** 1491-1509. doi:10.1080/01496395.2020.1784943.

ARONU, U. E., GONDAL, S., HESSEN, E. T., HAUG-WARBERG, T., HARTONO, A., HOFF, K. A. & SVENDSEN, H. F., 2011. Solubility of CO2 in 15, 30, 45 and 60 mass% MEA from 40 to 120 °C and model representation using the extended UNIQUAC framework. *Chem. Eng. Sci.,* 66**,** 6393-6406. doi:10.1016/j.ces.2011.08.042.

ASPEN TECHNOLOGY INC., 2014. Rate-Based Model of the CO2 Capture Process by MEA using Aspen Plus.

ASPEN TECHNOLOGY INC., 2019. Aspen Hysys, Version 11 [Computer program].

BARLOW, H., SHAHI, S. & KEARNS, D., 2025. Advancements in CCS technologies and costs. Global CCS Institute. Available: https://www.globalccsinstitute.com/wp-content/uploads/2025/08/Advancements-in-CCS-Technologies-and-Costs-Report-2.pdf (Accessed 24 March 2026).

BELABBACI, A., RAZZOUK, A., MOKBEL, I., JOSE, J. & NEGADI, L., 2009. Isothermal Vapor−Liquid Equilibria of (Monoethanolamine + Water) and (4-Methylmorpholine + Water) Binary Systems at Several Temperatures. *J. Chem. Eng. Data,* 54**,** 2312-2316. doi:10.1021/je800530u.

BILLET, R. & SCHULTES, M., 1999. Prediction of Mass Transfer Columns with Dumped and Arranged Packings. *Chem. Eng. Res. Des.,* 77**,** 498-504. doi:10.1205/026387699526520.

BÖTTINGER, W., MAIWALD, M. & HASSE, H., 2008. Online NMR spectroscopic study of species distribution in MEA-H2O-CO2 and DEA-H2O-CO2. *Fluid Phase Equilib.,* 263**,** 131-143. doi:10.1016/j.fluid.2007.09.017.

BRAVO, J. L., ROCHA, J. A. & FAIR, J. R., 1985. MASS TRANSFER IN GAUZE PACKINGS. *Hydrocarbon processing.,* 64**,** 91-95.

BUI, M., FLØ, N. E., DE CAZENOVE, T. & MAC DOWELL, N., 2020. Demonstrating flexible operation of the Technology Centre Mongstad (TCM) CO2 capture plant. *Int. J. Greenh. Gas Con.,* 93. doi:10.1016/j.ijggc.2019.102879.

CHAPEL, D. G., MARIZ, C. L. & ERNEST, J. Recovery of CO2 from Flue Gases: Commercial Trends. Canadian society of chemical engineers annual meeting. Vol. 4, 1999 Saskatoon, Canada.

CLARKE, L., WEI, Y.-M., NAVARRO, A. D. L. V., GARG, A., HAHMANN, A. N., KHENNAS, S., AZEVEDO, I. M. L., LÖSCHEL, A., SINGH, A. K., STEG, L., STRBAC, G. & WADA, K., 2022. Energy Systems. In IPCC, 2022: Climate Change 2022: Mitigation of Climate Change. Contribution of Working Group III to the Sixth Assessment Report of the

Intergovernmental Panel on Climate Change [P.R. Shukla, J. Skea, R. Slade, A. Al Khourdajie, R. van Diemen, D. McCollum, M. Pathak, S. Some, P. Vyas, R. Fradera, M. Belkacemi, A. Hasija, G. Lisboa, S. Luz, J. Malley, (eds.)]. Cambridge University Press, Cambridge, UK and New York, NY, USA. doi: 10.1017/9781009157926.008.

DE JOANNIS, P., CASTEL, C., KANNICHE, M., FAVRE, E. & AUTHIER, O., 2025. Direct Air Capture by Monoethanolamine Absorption with Heat Pump Enhancements. *Ind. Eng. Chem. Res.,* 64**,** 2208-2225. doi:10.1021/acs.iecr.4c02033.

DE KOEIJER, G., ENGE, Y., SANDEN, K., GRAFF, O. F., FALK-PEDERSEN, O., AMUNDSEN, T. & OVERÅ, S., 2011. CO2 Technology Centre Mongstad–Design, functionality and emissions of the amine plant. *Energy Proced.,* 4**,** 1207-1213. doi:10.1016/j.egypro.2011.01.175.

DHAKAL, S., MINX, J. C., TOTH, F. L., ABDEL-AZIZ, A., MEZA, M. J. F., HUBACEK, K., JONCKHEERE, I. G. C., KIM, Y.-G., NEMET, G. F., PACHAURI, S., TAN, X. C. & WIEDMANN, T., 2022. Emissions Trends and Drivers. In IPCC, 2022: Climate Change 2022: Mitigation of Climate Change. Contribution of Working Group III to the Sixth Assessment Report of the Intergovernmental Panel on Climate Change [P.R. Shukla, J. Skea, R. Slade, A. Al Khourdajie, R. van Diemen, D. McCollum, M. Pathak, S. Some, P. Vyas, R. Fradera, M. Belkacemi, A. Hasija, G. Lisboa, S. Luz, J. Malley, (eds.)]. Cambridge University Press, Cambridge, UK and New York, NY, USA. doi: 10.1017/9781009157926.004.

DU, Y., GAO, T., ROCHELLE, G. T. & BHOWN, A. S., 2021. Zero- and negative-emissions fossil-fired power plants using CO2 capture by conventional aqueous amines. *Int. J. Greenh. Gas Con.,* 111. doi:10.1016/j.ijggc.2021.103473.

DUGAS, R. 2009. *Carbon Dioxide Absorption, Desorption, and Diffusion in Aqueous Piperazine and Monoethanolamine. PhD Dissertation.* PhD, University of Texas at Austin.

DUGAS, R. & ROCHELLE, G., 2009. Absorption and desorption rates of carbon dioxide with monoethanolamine and piperazine. *Energy Proced.,* 1**,** 1163-1169. doi:10.1016/j.egypro.2009.01.153.

EDWARDS, T. J., MAURER, G., NEWMAN, J. & PRAUSNITZ, J. M., 1978. Vapor-liquid equilibria in multicomponent aqueous solutions of volatile weak electrolytes. *AIChE Journal,* 24**,** 966-976. doi:10.1002/aic.690240605.

FARAMARZI, L., THIMSEN, D., HUME, S., MAXON, A., WATSON, G., PEDERSEN, S., GJERNES, E., FOSTÅS, B. F., LOMBARDO, G., CENTS, T., MORKEN, A. K., SHAH, M. I., DE CAZENOVE, T. & HAMBORG, E. S., 2017. Results from MEA Testing at the CO2 Technology Centre Mongstad: Verification of Baseline Results in 2015. *Energy Proced.,* 114**,** 1128-1145. doi:10.1016/j.egypro.2017.03.1271.

FLUOR, 2004. Improvement in power generation with post-combustion capture of CO2. Report Number PH4/33. International Energy Agency Grenhouse Gas R&D Programme.

GOVERNMENT OF CANADA, 2024. Clean Electricity Regulations (SOR/2024-263). Available: https://laws-lois.justice.gc.ca/eng/regulations/SOR-2024-263/index.html (Accessed 13 March 2026).

HERZOG, H., 1999. An Introduction to CO2 Separation and Capture Technologies. MIT Energy Laboratory. Available: https://sequestration.mit.edu/pdf/introduction_to_capture.pdf (Accessed 11 July 2025).

HIKITA, H., ASAI, S., ISHIKAWA, H. & HONDA, M., 1977. The kinetics of reactions of carbon dioxide with monoethanolamine, diethanolamine and triethanolamine by a rapid mixing method. *Chem. Eng. J.,* 13**,** 7-12. doi:10.1016/0300-9467(77)80002-6.

HILLIARD, M. 2008. *A Predictive Thermodynamic Model for an Aqueous Blend of Potassium Carbonate, Piperazine, and Monoethanolamine for Carbon Dioxide Capture from Flue Gas.* PhD, The University of Texas at Austin.

JOU, F. Y., MATHER, A. E. & OTTO, F. D., 1995. The solubility of CO2 in a 30 mass percent monoethanolamine solution. *Can. J. Chem. Eng.,* 73**,** 140-147. doi:10.1002/cjce.5450730116.

LEE, J. I., OTTO, F. D. & MATHER, A. E., 1976. EQUILIBRIUM BETWEEN CARBON DIOXIDE AND AQUEOUS MONOETHANOLAMINE SOLUTIONS. *J. Appl. Chem. Biotechnol.,* 26**,** 541-549. doi:10.1002/jctb.5020260177.

LUO, X. & WANG, M., 2017. Improving Prediction Accuracy of a Rate-Based Model of an MEA-Based Carbon Capture Process for Large-Scale Commercial Deployment. *Engineering,* 3**,** 232-243. doi:10.1016/j.Eng.2017.02.001.

MA'MUN, S., NILSEN, R., SVENDSEN, H. F. & JULIUSSEN, O., 2005. Solubility of Carbon Dioxide in 30 mass % Monoethanolamine and 50 mass % Methyldiethanolamine Solutions. *J. Chem. Eng. Data,* 50**,** 630-634. doi:10.1021/je0496490.

MICHAILOS, S. & GIBBINS, J., 2022. A Modelling Study of Post-Combustion Capture Plant Process Conditions to Facilitate 95–99% CO2 Capture Levels From Gas Turbine Flue Gases. *Front. Energy Res.,* 10. doi:10.3389/fenrg.2022.866838.

MOKHATAB, S., POE, W. A. & MAK, J. Y., 2019. 'Chapter 7 - Natural Gas Treating'. *Handbook of Natural Gas Transmission and Processing.* Waltham, Mass.: Gulf Professional Publishing.

MORGAN, J. 17 June 2024. *RE: Query about Interfacial area in CCSI.* Email to MICHAILOS, S.

MORGAN, J. C., SOARES CHINEN, A., OMELL, B., BHATTACHARYYA, D., TONG, C., MILLER, D. C., BUSCHLE, B. & LUCQUIAUD, M., 2018. Development of a Rigorous Modeling Framework for Solvent-Based CO2 Capture. Part 2: Steady-State Validation and Uncertainty Quantification with Pilot Plant Data. *Ind. Eng. Chem. Res.,* 57**,** 10464-10481. doi:10.1021/acs.iecr.8b01472.

MORTON, F., LAIRD, R. & NORTHINGTON, J., 2013. The National Carbon Capture Center: Cost-effective test bed for carbon capture R&D. *Energy Proced.,* 37**,** 525-539. doi:10.1016/j.egypro.2013.05.139.

MULLEN, D. & LUCQUIAUD, M., 2024. On the cost of zero carbon electricity: A techno-economic analysis of combined cycle gas turbines with post-combustion CO2 capture. *Energy Rep.,* 11**,** 5104-5124. doi:10.1016/j.egyr.2024.04.067.

NOTZ, R., MANGALAPALLY, H. P. & HASSE, H., 2012. Post combustion CO2 capture by reactive absorption: Pilot plant description and results of systematic studies with MEA. *Int. J. Greenh. Gas Con.,* 6**,** 84-112. doi:10.1016/j.ijggc.2011.11.004.

PETRA NOVA, 2020. W.A. Parish Post-Combustion CO2 Capture and Sequestration Demonstration Project. Report DOE-PNPH-03311. Final Scientific/Technical Report. PETRA NOVA PARISH HOLDINGS LLC. Available: https://doi.org/10.2172/1608572 (Accessed 19 January 2023).

PINSENT, B. R. W., PEARSON, L. & ROUGHTON, F. J. W., 1956. The kinetics of combination of carbon dioxide with hydroxide ions. *Trans. Faraday Society,* 52**,** 1512-1520. doi:10.1039/tf9565201512.

RIAHI, K., SCHAEFFER, R., ARANGO, J., CALVIN, K., GUIVARCH, C., HASEGAWA, T., JIANG, K., KRIEGLER, E., MATTHEWS, R., PETERS, G. P., RAO, A., ROBERTSON, S., SEBBIT, A. M., STEINBERGER, J., TAVONI, M. & VAN VUUREN, D. P., 2022. Mitigation pathways compatible with long-term goals. In IPCC, 2022: Climate Change 2022: Mitigation of Climate Change. Contribution of Working Group III to the Sixth Assessment Report of the Intergovernmental Panel on Climate Change [P.R. Shukla, J. Skea, R. Slade, A. Al Khourdajie, R. van Diemen, D. McCollum, M. Pathak, S. Some, P. Vyas, R. Fradera, M. Belkacemi, A. Hasija, G. Lisboa, S. Luz, J. Malley, (eds.)]. Cambridge University Press, Cambridge, UK and New York, NY, USA. doi: 10.1017/9781009157926.005.

SHEN, K. P. & LI, M. H., 1992. Solubility of Carbon Dioxide in Aqueous Mixtures of Monoethanolamine with Methyldiethanolamine. *J. Chem. Eng. Data,* 37**,** 96-100. doi:10.1021/je00005a025.

SOARES CHINEN, A., MORGAN, J. C., OMELL, B., BHATTACHARYYA, D., TONG, C. & MILLER, D. C., 2018. Development of a Rigorous Modeling Framework for Solvent-Based CO2 Capture. 1. Hydraulic and Mass Transfer Models and Their Uncertainty Quantification. *Ind. Eng. Chem. Res.,* 57**,** 10448-10463. doi:10.1021/acs.iecr.8b01471.

SONG, D., SEIBERT, A. F. & ROCHELLE, G. T., 2018. Mass Transfer Parameters for Packings: Effect of Viscosity. *Ind. Eng. Chem. Res.,* 57**,** 718-729. doi:10.1021/acs.iecr.7b04396.

THOMPSON, J. A. & TSOURIS, C., 2021. Rate-Based Absorption Modeling for Postcombustion CO2 Capture with Additively Manufactured Structured Packing. *Ind. Eng. Chem. Res.,* 60**,** 14845-14855. doi:10.1021/acs.iecr.1c02756.

TOBIESEN, F. A., SVENDSEN, H. F. & JULIUSSEN, O., 2007. Experimental validation of a rigorous absorber model for CO2 postcombustion capture. *AIChE Journal,* 53**,** 846-865. doi:10.1002/aic.11133.

TONG, D. 2012. *Development of Advanced Amine Systems with Accurate Vapour-liquid Equilibrium Measurement.* Doctor of Philosophy, Imperial College London.

TREESE, S. A., 2015. Hydrogen Production and Management for Petroleum Processing. *Handbook of Petroleum Processing.* 2nd ed. Available: https://doi.org/10.1007/978-3-319-05545-9 (Accessed 18 November 2021): Springer International Publishing.

TSAI, R. 2010. *Mass Transfer Area of Structured Packing. PhD Dissertation.* PhD, University of Texas at Austin.

TSAI, R. E., SEIBERT, A. F., ELDRIDGE, R. B. & ROCHELLE, G. T., 2011. A dimensionless model for predicting the mass-transfer area of structured packing. *AIChE Journal,* 57**,** 1173-1184. doi:10.1002/aic.12345.

UHRIG, L. 25 September 2025. *RE: PSTU with storage.* Email to GIBBINS, J.

UK ENVIRONMENT AGENCY, 2024. Guidance. Post-combustion carbon dioxide capture: emerging techniques. Available: https://www.gov.uk/guidance/post-combustion-carbon-dioxide-capture-best-available-techniques-bat (Accessed 28 June 2024).

XU, Q. & ROCHELLE, G., 2011. Total pressure and CO2 solubility at high temperature in aqueous amines. *Energy Proced.,* 4**,** 117-124. doi:10.1016/j.egypro.2011.01.031.

ZHANG, Y. & CHEN, C.-C., 2013. Modeling CO2 Absorption and Desorption by Aqueous Monoethanolamine Solution with Aspen Rate-based Model. *Energy Proced.,* 37**,** 1584-1596. doi:10.1016/j.egypro.2013.06.034.

ZHANG, Y., CHEN, H., CHEN, C.-C., PLAZA, J. M., DUGAS, R. & ROCHELLE, G. T., 2009. Rate-Based Process Modeling Study of CO2 Capture with Aqueous Monoethanolamine Solution. *Ind. Eng. Chem. Res.,* 48**,** 9233-9246. doi:10.1021/ie900068k.

Graphical abstract

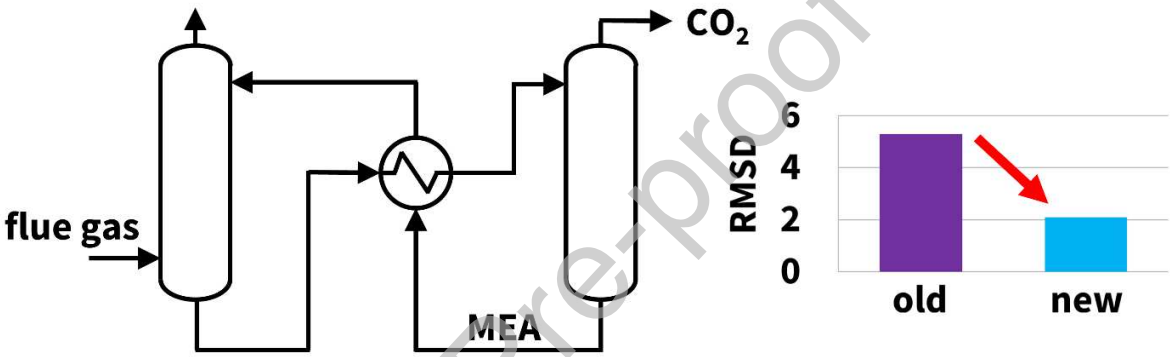


**Declaration of interests**

☒ The authors declare that they have no known competing financial interests or personal relationships that could have appeared to influence the work reported in this paper.